Research Article | Vol. 28, No. 5 / 2 March 2020 / Optics Express 6909

Optics EXPRESS

Direct integration of micro-LEDs and a SPAD detector on a silicon CMOS chip for data communications and time-of-flight ranging

J. F. C. Carreira,[1,*] A. D. Griffiths,[1] E. Xie,[1] B. J. E. Guilhabert,[1] J. Herrnsdorf,[1] R. K. Henderson,[2] E. Gu,[1] M. J. Strain,[1] and M. D. Dawson[1]

[1]Institute of Photonics, Department of Physics, University of Strathclyde, Glasgow G1 1RD, UK
[2]Institute for Integrated Micro and Nano Systems, School of Engineering, University of Edinburgh, Edinburgh EH9 3FF, UK
[*]jose.correia-carreira@strath.ac.uk

Abstract: We present integration of singulated micron-sized light emitting diodes (micro-LEDs) directly onto a silicon CMOS drive chip using a transfer printing method. An 8x8 micro-LED device array with individual control over each pixel is demonstrated with modulation bandwidths up to 50 MHz, limited by the large modulation depth of the driver chip. The 2 kHz frame rate CMOS driver also incorporates a Single Photon Avalanche Diode device thus allowing detection and transmission functionality on a single integrated chip. Visible light communications at data rates up to 1 Mbps, and time-of-flight ranging with cm-scale resolution are demonstrated using this hybrid integrated system.

1. Introduction

Arrays of micron-sized light emitting diodes (micro-LEDs or μLEDs) on sapphire substrates can be directly integrated with their electronic drive chips using standard flip-chip bonding processes [1,2], producing individually addressable, high-speed sources for visible light communications (VLC) [3] and spatial navigation [4] in compact, chip-scale systems. The transparency of sapphire at typical III-N emission wavelengths allows for vertical emission of individual pixels through the substrate. Patterning of lenses [5] and surface features [6] allows for enhanced emission out of the substrate bulk. However, flip-chip integration can result in issues with uniformity in the emission from large arrays due to the bump bonding process, and multiple reflection paths within the substrate can lead to cross-talk between pixels. Furthermore, flip-chip bonding is not suitable in cases where the device emission, or detection, wavelength is absorbed by the flipped substrate. An alternative integration technique is micro-transfer printing (μTP), where individual thin film devices are removed from their growth substrate and transferred onto a host chip, using an accurate form of pick and place [7]. This technique allows the population of the host substrate with devices only where required, removing issues associated with a flip-chipped substrate. This method has been shown to be able to handle micro-LED chips as small as 8x15 μm^2, with extremely high-yield [8], and has been used to realise, for example, micro-displays on flexible substrates [9] or optical gain on silicon photonics [10]. In addition to the printing of optically active devices, direct integration of optical and electronic layers has been demonstrated on flexible substrates [11]. Nevertheless, the majority of transfer printed systems use electronic tracks and wire-bonds to connect the optical devices to their respective drive electronics, limiting the potential for dense integration and compact system geometries.

#384746 https://doi.org/10.1364/OE.384746
Journal © 2020 Received 12 Dec 2019; revised 10 Jan 2020; accepted 12 Feb 2020; published 24 Feb 2020

Optics EXPRESS

In this work, we present the integration of nitride micro-LED devices directly onto silicon (Si)-CMOS drive chips. Micro-LED platelets are fabricated on their native Si substrate and then transfer printed onto pixels of a CMOS chip for individual control over each pixel. An 8x8 array of devices is realised with operation bandwidths in the 10's of MHz range, with excellent uniformity both in brightness and modulation performance across the pixel array. High-speed optical camera communications (OCC) are demonstrated using spatio-temporal modulation of the array. The silicon driver chip also includes a Single Photon Avalanche Diode (SPAD) device that allows the single chip to act as a transceiver. Demonstration of data communications and time-of-flight (ToF) ranging operation, using the SPAD as a receiver, is presented.

2. Micro-LED fabrication and integration onto CMOS by μTP

Blue (450 nm) top-emitting through the *p*-GaN micro-LED platelets were fabricated from commercial InGaN LED epistructures, grown on a Si 111-oriented substrate, following conventional microfabrication procedures [12]. The LED epitaxial structure comprises a 200 nm thick aluminum nitride (AlN) layer, followed by a 950 nm Al-graded GaN buffer layer, an 800 nm thick *n*-doped GaN, a 100 nm thick multi-quantum well (MQW) layer, and a 140 nm thick *p*-doped GaN layer (Fig. 1(a1)). In the first fabrication step, a nickel/gold (Ni/Au thicknesses 10/20 nm) bilayer was electron beam deposited, lithographically patterned, and annealed in an air environment at 510 ° C defining a semitransparent *p*-GaN metal contact (Fig. 1(a2)). Inductively coupled plasma (ICP) etching was used to expose the underlying *n*-GaN layer, thus defining a $6.5\text{x}10^{-5}$ cm^2 active area pixel (Fig. 1(a3)). Another ICP etch step down to the Si(111) substrate created a 100x100 μm^2 mesa and exposed the chemically preferentially etched Si(110) planes (Fig. 1(a4)). In order to fabricate suspended transferable micro-LED platelets, supporting "anchors", which tether the micro-LED platelet to the Si substrate, were also defined during the ICP mesa etching. The Si (110) planes, underneath the micro-LED platelets, were anisotropically etched away in a 30% potassium hydroxide solution at 80 °C (Fig. 1(a5)). Upon completion of this etching step, the micro-LED platelets are held suspended above an air gap (2 μm), by two sacrificial supporting "anchors" [13].

The CMOS chip was implemented in standard 0.35 μm CMOS technology and consists of a 16x16 array of individually-controllable 100x100 μm^2 p-MOS driver cells on a center-to-center pitch of 100 μm (backplane driver circuit shown in [14]). This chip was custom designed to be integrated with on-sapphire 16x16 micro-LED arrays by conventional gold bump flip-chip bonding. Integrated devices using this driver chip have been demonstrated for VLC [3], spatial navigation [4], and OCC [15]. In addition to the 16x16 main array of driver pixels, the CMOS chip also contains a single free running SPAD. The SPAD, which has a dead time of 40 ns (saturation of 25 MHz) and active area diameter of 6 μm (further details and pixel circuit in [16]) is an avalanche photodiode operating in Geiger mode, providing digital pulses on the detection of a single photon. The potential is therefore available for a single chip, with suitable optical bonded devices, to act as both an optical transmitter and receiver.

An 8x8 array of micro-LEDs was sequentially transfer printed directly, without any adhesion enhancement layer, onto the CMOS drivers. An elastomeric polydimethylsiloxane (PDMS) stamp, with pyramidal protrusions, was used to pick-up the suspended micro-LED platelets from their Si substrate (Fig. 1(b)) and print them onto every other CMOS drivers (Fig. 1(c)) [13]. Since the micro-LED mesa is the same size as the CMOS driver and the micro-LED backside is non-conductive, the adjacent CMOS driver was used to address each respective micro-LED. For this purpose, after μTP of the micro-LEDs, a parylene-C (Pa-c) layer (thickness 4.5 μm) was deposited and apertures on the micro-LED contacts and CMOS drivers were lithographically defined. Next, titanium/gold (Ti/Au thicknesses 100/200 nm) metal tracks were lithographically defined, connecting the p-MOS driver to the micro-LED *p*-contact and the micro-LED *n*-contact to the common ground. Figure 1(d) shows a schematic cross-section view of the micro-LED

Optics EXPRESS

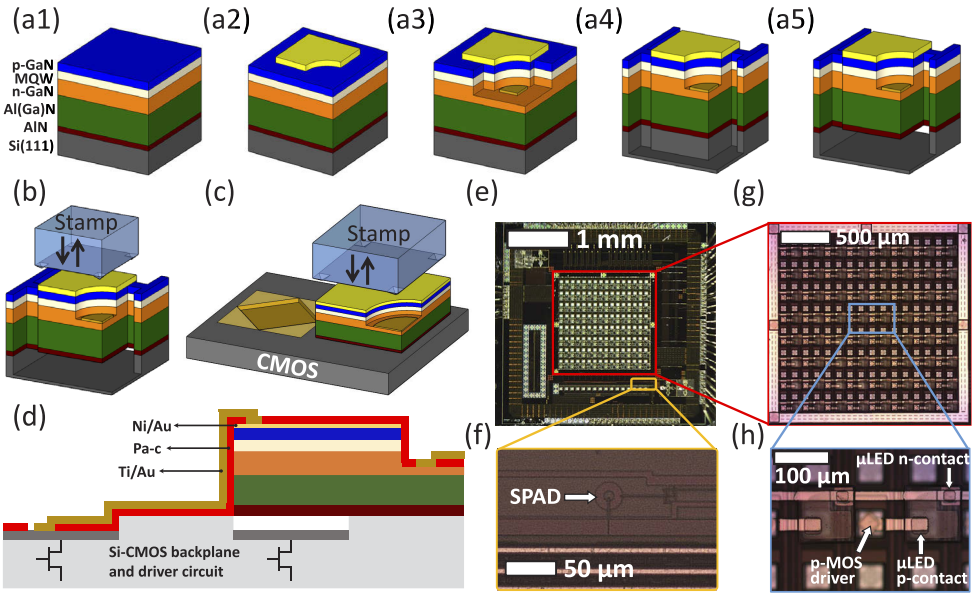

Fig. 1. (a) Schematic drawings of the micro-LED platelets fabrication process (not to scale, see text for further details); (b) and (c) schematic drawing of the transfer printing process during pick-up and printing of the micro-LED platelet, respectively; (d) schematic cross-section drawing of the finalised device; (e) optical image of the CMOS chip with the micro-LED active area and SPAD identified in red and yellow, respectively; (f) magnification showing in further detail the SPAD active area; (g) magnification of the CMOS chip showing the 8x8 array of transfer printed micro-LEDs; (h) shows, in further detail, the micro-LED *p*-GaN electrical connection through the adjacent p-MOS driver.

directly printed onto the CMOS. Figure 1(e) shows an optical image of the finalised device. Figure 1(f) shows in further detail the monolithic SPAD, while Figs. 1(g) and 1(h) show the full micro-LED array and the micro-LED electrical connecting scheme through the adjacent p-MOS driver, respectively.

3. Single micro-LED and full array performance

3.1. *Single micro-LED electrical, optical, and bandwidth performance*

Figure 2(a) shows the current density *vs* voltage, J-V, and optical power density *vs* current density, L-J, characteristics of a representative micro-LED in the 8x8 CMOS-driven array. The inset of Fig. 2(a) presents the electroluminescence (EL) spectrum acquired at 22.2 A/cm^2. The J-V characteristic was measured by a voltage source, through scanning each data point under direct current (DC) conditions (Yokogawa GS610). The L-J was measured using a calibrated Si photodiode detector (9 mm diameter active area, Thorlabs PM100D) placed in close proximity (5 mm) to the micro-LED topside. A Lambertian emission profile was assumed to convert the collected optical power into values quoted for the full forward hemisphere. The EL spectrum was acquired using an optical fiber-coupled spectrometer (Avantes AvaSpec-2048L spectrometer). The forward diode voltage of commercial LED's (250x250 μm^2 size) is usually defined at 20 mA, corresponding to a current density of 32 A/cm^2 [17]. At this current density the CMOS-driven micro-LED, reported in this work, exhibits a forward voltage of 3.65 V. The micro-LED presents an optical power density of 11 W/cm^2, at 161 A/cm^2, which translates into a brightness of 7.79x10^5 cd/m^2. The EL spectrum is composed of one major peak centred at 450 nm and

Optics EXPRESS

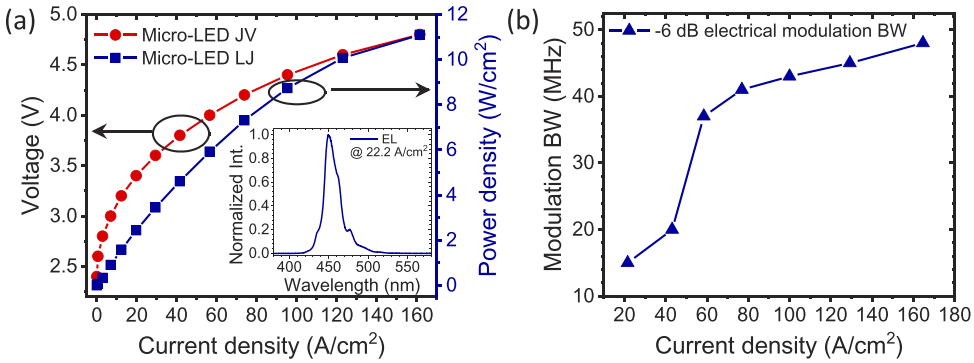

Fig. 2. (a) CMOS-driven micro-LED current density *vs* voltage (JV) curve, current density *vs* optical power density (LJ) curve, and electroluminescence spectra (EL); (b) CMOS-driven micro-LED -6 dB electrical modulation bandwidth *vs* current density.

broadened by Fabry-Perot interference occurring due to high refractive index contrast between the GaN epilayers and air [13].

The -6 dB electrical modulation bandwidth of the CMOS-driven micro-LED was measured using a network analyzer (HP8753ES) and a Si avalanche photodetector (Thorlabs — APD430A2/M bandwidth 400 MHz). As the CMOS driver is a digital device, 1 V peak-to-peak output from the network analyzer was combined with a DC offset (1.5 V) to reach the logic threshold of the electronics and then sent to the CMOS driver board through an SMA connector to modulate the corresponding micro-LED. This results in a square wave driving signal for the micro-LED, modulating between 0 V and an adjustable micro-LED bias voltage. The optical output of the micro-LED was then lens-focused onto the detector and the electrical output of the detector was fed back to the network analyzer. The modulation bandwidth of the CMOS-driven micro-LED, at different current densities, is shown in Fig. 2(b). The CMOS-driven micro-LED exhibits a modulation bandwidth of 48 MHz at 165 A/cm^2, which is lower than a comparable transfer printed micro-LED packaged on a printed circuit board (PCB) [18]. This is attributed to the high modulation depth of the CMOS driver output [3].

3.2. *Micro-LED array performance*

The micro-LED yield and uniformity of electrical/optical characteristics across the full array are important factors for applications. The reported μTP-enabled hybridization process exhibits a 100% yield, with 64 out of 64 operational micro-LEDs. No electrical crosstalk has been observed showing a suitable insulation and electrical contact scheme. In addition, as each micro-LED is a singulated device, no optical crosstalk between neighbouring micro-LEDs has been observed.

Figures 3(a) and 3(b) show a “heat map" distribution of the forward voltage (defined at 32 A/cm^2) and optical power density at 60 A/cm^2 across the full array, respectively. The mean and standard deviation values for the forward voltage and power density are 3.9 ± 0.3 V and 6 ± 1 W/cm^2, respectively. The most erratic values originate from column 1 row 6 and column 1 row 7, which exhibit some electrical leakage behavior. Similar electrical leakage behavior has also been observed on micro-LEDs μTP onto a glass substrate [19]. It has been suggested that this is due to damage to the device sidewalls occurring when the Si substrate is removed, leaving a rough surface and increasing opportunities for tunneling. This can be further investigated by topographic and conductive atomic force microscopy and scanning Kelvin probe microscopy [20]. Nevertheless, these pixels are fully operational and can be used in practical applications as detailed in the following results. In addition, the bandwidth of 5 randomly selected CMOS-driven micro-LEDs at 4.6 V forward bias was found to be of high uniformity: 44.8 ± 0.5 MHz.

Optics EXPRESS

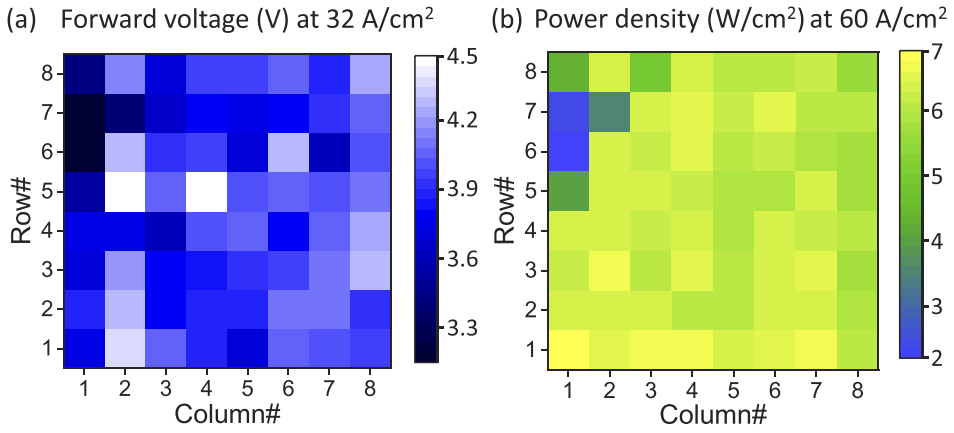

Fig. 3. "Heat map" distribution of (a) forward voltage and (b) optical power density at 60 A/cm^2 across the full array.

In order to demonstrate that the μTP-enabled hybridization process does not physically damage the CMOS, operation of the CMOS-driven micro-LED array as a transmitter in an OCC link is demonstrated. This has previously been demonstrated with a flip-chip bonded array in Ref. [15], however uniformity issues and faulty pixels in the array were a significant cause of errors in transmission. With the μTP device, yield and uniformity are significantly improved, so better results are expected. For this the CMOS-driven micro-LED array was DC biased at 4.6 V (average total current of 12.5 mA) producing an average total optical power of 2.77 mW. The patterns were updated at a rate of 2 kHz, being only limited by the full-array refresh rate of the CMOS electronics [4]. Thus each micro-LED pixel is transmitting independent binary data at 2 kHz, resulting in a net data rate of 2000x8x8=128 kbps. 4 blocks of 67 frames (a total of 268 frames) are transmitted with an overhead of 4.48% (3 frames in every 67) for synchronisation, and determining thresholds and alignment. This overhead can be reduced, depending on the number of data frames per transmitted block. A pseudorandom sequence of 2^{14} useful bits were transmitted in order to measure a bit-error-ratio (BER). The emitted light was lens-focused

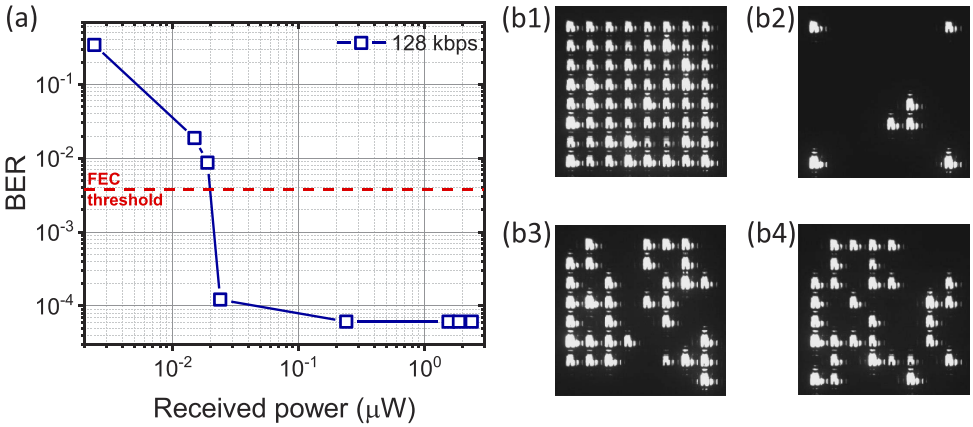

Fig. 4. (a) Bit-error-ratio (BER) measured as a function of received power by the ultrafast camera; (b1)–(b4) show the captured frames from the 8000 fps video for all active micro-LEDs, alignment conditions, and two different pseudo-random patterns, respectively.

Optics EXPRESS

(Nikon Plan Fluor 4x/0.13) onto an ultrafast camera (Photron Fastcam UX100). The camera acquisition parameters were set at 8000 frames per second (fps), resolution of 1280x616, and a total acquisition time of 302 ms. Figure 4(a) shows the BER as a function of the received power by the camera. The received power was changed by placing different neutral density filters at the receiver. The BER floor of $6.10\text{x}10^{-5}$ ($1/2^{14}$) occurs as 2^{14} total bits were transmitted, so a lower BER cannot be measured. For optical power values lower than 0.02 μW the BER is larger than the $3.8\text{x}10^{-3}$ limit for forward error correction (FEC) coding [21]. Example image frames for the full array, alignment frame and two example data frames are shown in Figs. 4(b1)–4(b4), respectively.

4. On-chip single micro-LED/SPAD operation

The multifunctional capability of the μTP-enabled CMOS-driven integrated emitter and receiver, has been demonstrated by its application as an optical communication transceiver and ToF ranging device. A single μTP DC biased micro-LED pixel was used for both experiments. It was experimentally verified that the on-chip crosstalk between the micro-LED and SPAD is insignificant, and therefore it is impossible to establish a direct detection link without additional optics. Thus, the μTP micro-LED (identified in red - Fig. 5(a)) light was lens-collected, back reflected, and focused onto the SPAD (identified in yellow - Fig. 5(a)). This setup provides an estimation of the device performance as an integrated transceiver. Figure 5(b) shows a schematic drawing of the input electrical signal for the VLC and ToF ranging experiments.

4.1. VLC transceiver

In the first demonstration a free-space VLC link is implemented. For this, the micro-LED was modulated with an on-off signal provided by an FPGA module (Opal Kelly XEM6310-LX45) and applied to the CMOS control electronics. An aspheric lens (Thorlabs ACL25416U-A) was used to approximately collimate the emission. The light was reflected by a mirror at a distance of approximately 2 cm, and transmitted back through the lens. The angle of the mirror was adjusted to focus the light back on to the SPAD, which is laterally ~2 mm away from the emitting micro-LED. The output signal from a SPAD is a series of digital pulses indicating the detection of a photon, including noise and dark counts. Therefore, to produce a meaningful data signal, counts must be summed over a time interval. Photon counts per data period can then be compared to a threshold value to decode a data signal. The output of the SPAD was captured by an oscilloscope and processed offline in MATLAB. A pseudorandom bit sequence of length 2^{12} bits was transmitted, and repeated to transmit a total of over $4\text{x}10^4$ bits, sufficient to justify a BER of less than $1\text{x}10^{-4}$. Figure 6(a) shows the BER as a function of incident power on the SPAD. VLC links of 500 kbps and 1 Mbps, below the FEC threshold, are demonstrated. For the 500 kbps link, communication, below FEC, is possible down to 58 pW of incident power. By increasing the data rate to 1 Mbps the minimum incident power for communication below the

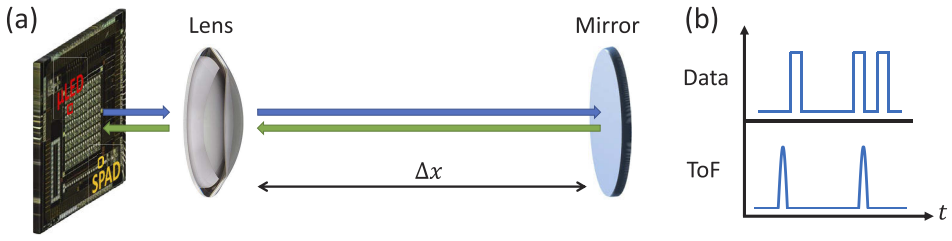

Fig. 5. (a) Schematic drawing of the experimental setup used in VLC ($\Delta x \sim 2$ cm) and ToF ranging ($\Delta x = 0 : 0.2 : 1.2$ m) demonstrations; (b) Schematic drawing of the input electrical signal for the VLC and ToF experiments.

Optics EXPRESS

FEC limit is 135 pW.

4.2. Time-of-flight ranging

To demonstrate ranging capability, the micro-LED was operated in a pulsed manner. The FPGA module was used to generate 20 ns wide electrical pulses at a repetition rate of 3.13 MHz. This rate was chosen as a compromise between rapid acquisition of ranging data and the ability to fully resolve individual pulses. As the CMOS and the micro-LED bandwidth limit the rise and fall times, applying this signal to the CMOS driver generates optical pulses from the micro-LED with a full width at half maximum of 19 ns. An aspheric lens (Thorlabs ACL50832U-A) was used to collimate the micro-LED output. A large mirror (COMAR 250 MC 160) was used to reflect the light back to the chip and refocus on to the SPAD. The distance from the CMOS chip to the mirror was changed from 0 to 1.2 m in 0.2 m intervals. The SPAD output was used as the start signal to trigger a time-to-digital converter (Texas Instruments TDC7200), with a stop signal provided by the FPGA module. Thus, time of flight for single photons is recorded using reverse time-correlated single photon counting (TCSPC) methods [22]. By repeating the single photon arrival time measurements and building up a histogram, the optical pulse shape is recovered, and time of flight can be measured by finding the centroid of the received peak [23]. For these experiments, 10^4 arrival times were measured in dark laboratory conditions. Using a repetition rate of 3.13 MHz (*Rep*) and 10^4 samples (N) gives an acquisition time (T) of ~3 ms ($T = N/Rep$), which provides an adequate capture for simple time of flight ranging. In addition, at this repetition rate, an effective accessible range (i.e. spatial pulse separation divided by two) of 48 m is achieved. The resulting distance measurements are shown in Fig. 6(b), along with the histogram acquired at 1.2 m. While the precision is limited by the width of the optical pulses, this proof-of-concept demonstration shows cm-scale distance measurements over a 1.2 m distance with a root-minimum-square (RMS) deviation of 8.14 cm.

5. Conclusion

In conclusion, we have demonstrated the direct integration of an 8x8 array of GaN-based micro-LEDs onto CMOS circuitry by micro-transfer printing, without any adhesion-enhancement layer. A representative CMOS-driven micro-LED exhibits a forward diode voltage of 3.65 V and an optical power density of 11 W/cm^2 at 161 A/cm^2. The CMOS-driven micro-LED modulation bandwidth of 48 MHz at 165 A/cm^2 is limited by the CMOS driver and its high modulation depth output. The reported μTP-enabled integration process exhibits a 100% yield with mean

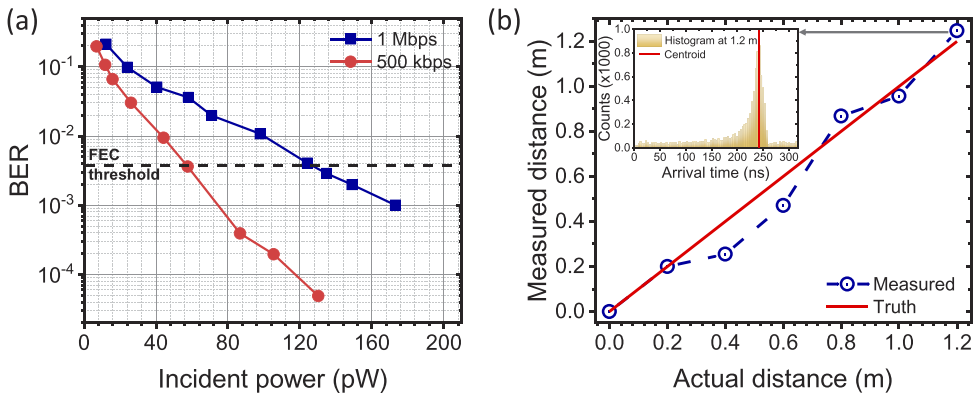

Fig. 6. (a) Bit-error-ratio (BER) measured as a function of the incident power on the SPAD; (b) measured distance plotted as a function of the actual distance in a ranging setup (inset shows the histogram acquired at 1.2 m).

Optics EXPRESS

and standard deviation values for the forward voltage and power density, across the full array, of 3.9 ± 0.3 V and 6 ± 1 W/cm^2, respectively. The high yield and uniformity led to a demonstration of a 128 kbps OCC link below BER for optical power larger than 0.02 μW. On-chip excitation and detection enabled the demonstration of an 1 Mbps VLC link and ToF ranging up to 1.2 m with a RMS deviation of 8.14 cm.

Due to its low temperature and minimal mechanical pressure the μTP-enabled integration process can be extended to a wide range of materials/devices. In particular, the integration of full color micro-emitters onto CMOS is highly sought for virtual/augmented reality applications, and can be achieved using the techniques demonstrated here. Furthermore, we envisage the hybrid integration of micro-LEDs and SPAD, shown in this work, to find further applications in single chip architecture, low size, weight, power and cost (SWaP-C) VLC transceivers and ToF ranging devices.

Supporting data can be found at https://doi.org/10.15129/718b2ab0-16fe-43eb-9a4c-490c01ad0b29.

Funding

Engineering and Physical Sciences Research Council (EP/T00097X/1, EP/R03480X/1, EP/S001751/1).

Acknowledgments

Plessey Semiconductors Ltd. is acknowledged for providing the GaN-on-Si wafer.

Disclosures

The authors declare no conflicts of interest.

References

1. J. J. D. McKendry, B. R. Rae, Z. Gong, K. R. Muir, B. Guilhabert, D. Massoubre, E. Gu, D. Renshaw, M. D. Dawson, and R. K. Henderson, "Individually Addressable AlInGaN Micro-LED Arrays With CMOS Control and Subnanosecond Output Pulses," IEEE Photonics Technol. Lett. **21**(12), 811–813 (2009).
2. J. Day, J. Li, D. Y. C. Lie, C. Bradford, J. Y. Lin, and H. X. Jiang, "III-Nitride full-scale high-resolution microdisplays," Appl. Phys. Lett. **99**(3), 031116 (2011).
3. S. Zhang, S. Watson, J. J. D. McKendry, D. Massoubre, A. Cogman, E. Gu, R. K. Henderson, A. E. Kelly, and M. D. Dawson, "1.5 Gbit/s Multi-Channel Visible Light Communications Using CMOS-Controlled GaN-Based LEDs," J. Lightwave Technol. **31**(8), 1211–1216 (2013).
4. J. Herrnsdorf, M. J. Strain, E. Gu, R. K. Henderson, and M. D. Dawson, "Positioning and Space-Division Multiple Access Enabled by Structured Illumination With Light-Emitting Diodes," J. Lightwave Technol. **35**(12), 2339–2345 (2017).
5. H. W. Choi, C. Liu, E. Gu, G. McConnell, J. M. Girkin, I. M. Watson, and M. D. Dawson, "GaN micro-light-emitting diode arrays with monolithically integrated sapphire microlenses," Appl. Phys. Lett. **84**(13), 2253–2255 (2004).
6. J.-Y. Cho, K.-J. Byeon, H. Park, J. Kim, H.-S. Kim, and H. Lee, "Improvement of photon extraction efficiency of GaN-based LED using micro and nano complex polymer structures," Nanoscale Res. Lett. **6**(1), 578 (2011).
7. A. Carlson, A. M. Bowen, Y. Huang, R. G. Nuzzo, and J. A. Rogers, "Transfer Printing Techniques for Materials Assembly and Micro/Nanodevice Fabrication," Adv. Mater. **24**(39), 5284–5318 (2012).
8. C. A. Bower, M. A. Meitl, B. Raymond, E. Radauscher, R. Cok, S. Bonafede, D. Gomez, T. Moore, C. Prevatte, B. Fisher, R. Rotzoll, G. A. Melnik, A. Fecioru, and A. J. Trindade, "Emissive displays with transfer-printed assemblies of 8 μm x 15 μm inorganic light-emitting diodes," Photonics Res. **5**(2), A23–A29 (2017).
9. S.-I. Park, Y. Xiong, R.-H. Kim, P. Elvikis, M. Meitl, D.-H. Kim, J. Wu, J. Yoon, C.-J. Yu, Z. Liu, Y. Huang, K.-c. Hwang, P. Ferreira, X. Li, K. Choquette, and J. A. Rogers, "Printed Assemblies of Inorganic Light-Emitting Diodes for Deformable and Semitransparent Displays," Science **325**(5943), 977–981 (2009).
10. J. Zhang, G. Muliuk, J. Juvert, S. Kumari, J. Goyvaerts, B. Haq, C. Op de Beeck, B. Kuyken, G. Morthier, D. Van Thourhout, R. Baets, G. Lepage, P. Verheyen, J. Van Campenhout, A. Gocalinska, J. OĆallaghan, E. Pelucchi, K. Thomas, B. Corbett, A. J. Trindade, and G. Roelkens, "III-V-on-Si photonic integrated circuits realized using micro-transfer-printing," APL Photonics **4**(11), 110803 (2019).

Optics EXPRESS

11. M. Choi, B. Jang, W. Lee, S. Lee, T. W. Kim, H.-J. Lee, J.-H. Kim, and J.-H. Ahn, "Stretchable Active Matrix Inorganic Light-Emitting Diode Display Enabled by Overlay-Aligned Roll-Transfer Printing," Adv. Funct. Mater. **27**(11), 1606005 (2017).
12. P. Tian, J. J. D. McKendry, Z. Gong, S. Zhang, S. Watson, D. Zhu, I. M. Watson, E. Gu, A. E. Kelly, C. J. Humphreys, and M. D. Dawson, "Characteristics and applications of micro-pixelated GaN-based light emitting diodes on Si substrates," J. Appl. Phys. **115**(3), 033112 (2014).
13. A. J. Trindade, B. Guilhabert, D. Massoubre, D. Zhu, N. Laurand, E. Gu, I. M. Watson, C. J. Humphreys, and M. D. Dawson, "Nanoscale-accuracy transfer printing of ultra-thin AlInGaN light-emitting diodes onto mechanically flexible substrates," Appl. Phys. Lett. **103**(25), 253302 (2013).
14. B. R. Rae, J. Yang, J. McKendry, Z. Gong, D. Renshaw, J. M. Girkin, E. Gu, M. D. Dawson, and R. K. Henderson, "A Vertically Integrated CMOS Microsystem for Time-Resolved Fluorescence Analysis," IEEE Transactions on Biomed. Circuits Syst. **4**(6), 437–444 (2010).
15. A. D. Griffiths, J. Herrnsdorf, M. J. Strain, and M. D. Dawson, "Scalable visible light communications with a micro-LED array projector and high-speed smartphone camera," Opt. Express **27**(11), 15585–15594 (2019).
16. C. Niclass, M. Sergio, and E. Charbon, "A Single Photon Avalanche Diode Array Fabricated in Deep-Submicron CMOS Technology," Proc. Des. Autom. Test Eur. Conf. **1**, 1–6 (2006).
17. E. F. Schubert, *Light-Emitting Diodes* (Cambridge University Press, 2006).
18. J. F. C. Carreira, E. Xie, R. Bian, C. Chen, J. J. D. McKendry, B. Guilhabert, H. Haas, E. Gu, and M. D. Dawson, "On-chip GaN-based dual-color micro-LED arrays and their application in visible light communication," Opt. Express **27**(20), A1517–A1528 (2019).
19. K. Rae, P. P. Manousiadis, M. S. Islim, L. Yin, J. Carreira, J. J. D. Mckendry, B. Guilhabert, I. D. W. Samuel, G. A. Turnbull, N. Laurand, H. Haas, and M. D. Dawson, "Transfer-printed micro-led and polymer-based transceiver for visible light communications," Opt. Express **26**(24), 31474–31483 (2018).
20. X. Cao, J. Teetsov, F. Shahedipour-Sandvik, and S. Arthur, "Microstructural origin of leakage current in GaN/InGaN light-emitting diodes," J. Cryst. Growth **264**(1-3), 172–177 (2004).
21. I. T. Union, "Forward error correction for high bit-rate DWDM submarine systems," ITU, Geneva, Switzerland, Tech. Rep. ITU-T G.975.1 (2013).
22. W. Becker, *Advanced Time-Correlated Single Photon Counting Techniques* (Springer Series in Chemical Physics, 2005).
23. A. D. Griffiths, H. Chen, D. D.-U. Li, R. K. Henderson, J. Herrnsdorf, M. D. Dawson, and M. J. Strain, "Multispectral time-of-flight imaging using light-emitting diodes," Opt. Express **27**(24), 35485–35498 (2019).